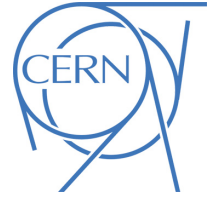




ATLAS CONF Note

ATLAS-CONF-2019-046

30th September 2019



Measurement of the top quark mass using a leptonic invariant mass in pp collisions at $\sqrt{s} = 13$ TeV with the ATLAS detector

The ATLAS Collaboration

A measurement of the top quark mass (m_t) in the $t\bar{t} \rightarrow \text{lepton} + \text{jets}$ channel is presented, with an experimental technique which exploits semileptonic decays of b -hadrons produced in the top-quark decay chain. The distribution of the invariant mass $m_{\ell\mu}$ between the lepton, ℓ (with $\ell = e, \mu$), from the W -boson decay and the muon, μ , originating from the b -hadron decay is reconstructed, and a binned-template profile likelihood fit is performed to extract m_t . The measured value of the top quark mass is $m_t = 174.48 \pm 0.40$ (stat) ± 0.67 (syst) GeV, based on data corresponding to an integrated luminosity of 36.1 fb^{-1} of $\sqrt{s} = 13$ TeV pp collisions provided by the Large Hadron Collider and recorded by the ATLAS detector.

ATLAS-CONF-2019-046
17 October 2019



1 Introduction

The large mass of the top quark plays a role in much of the dynamics of elementary particles via loop diagrams. Linked by the gauge structure of the Standard Model (SM), the large top quark mass affects very significantly the radiative corrections to the Higgs boson and W -boson masses, establishing a relationship that can be used for precision tests of the consistency of the SM [1]. Furthermore, a precise measurement of the top quark mass is required to predict the evolution of the Higgs quartic coupling at high scales [2] [3].

If performed with a precision of the order of a few hundred MeV, the direct reconstruction of the top quark mass from its decay products, and the indirect measurements from top quark production cross-sections or kinematic distributions, are important not only for the constraints mentioned above, but also because of the ambiguity and challenges offered by the theoretical interpretation of such measurements [4, 5].

In this paper, a direct measurement of the top quark mass (m_t) is presented using a technique that exploits a partial, leptonic-only, invariant mass reconstruction of the top-quark decay products. The analysis is performed from a sample of reconstructed $t\bar{t}$ events in the ℓ +jets channel. In the top-quark decay $t \rightarrow Wb$, the invariant mass $m_{\ell\mu}$ between the lepton ℓ (with $\ell = e, \mu$) from the W -boson decay and the muon μ from a semileptonic decay of a b -hadron, is constructed as the observable sensitive to the parent m_t value. The advantages of a strategy based on leptonic variables for the measurement of the top quark mass rest mainly on the smaller sensitivity to the jet energy calibration and energy resolution, compared to the standard direct reconstruction methods, and on less sensitivity to top-quark production modelling (owing to the boost-invariant construction) than in methods based on the W lepton alone. Furthermore, methods with different types of systematic uncertainties are important for combining measurements, and to test the consistency of the theoretical interpretation of the top quark mass.

The $m_{\ell\mu}$ distribution from models with different top quark mass hypotheses is compared to data, and the optimal value of m_t is determined from a binned-template profile likelihood fit. A similar technique was first employed by the CDF Collaboration at the Tevatron collider [6], and a closely-related analysis with J/ψ decays has been presented by the CMS Collaboration [7]; however both these analyses yielded uncertainties on m_t of several GeV. To date, the most precise measurement of the top quark mass in the $t\bar{t} \rightarrow \ell$ +jets channel by the ATLAS Collaboration is $m_t = 172.08 \pm 0.39(\text{stat}) \pm 0.82(\text{syst})$ GeV, whereas combining multiple ATLAS measurements gives $m_t = 172.69 \pm 0.48$ GeV [8]. The CMS Collaboration reports its most precise combination as $m_t = 172.44 \pm 0.48$ GeV [9], and the Tevatron experiments report a combined value of $m_t = 174.30 \pm 0.65$ GeV [10].

2 ATLAS experiment

The ATLAS experiment [11] at the LHC is a multipurpose particle detector with a forward–backward symmetric cylindrical geometry and a near 4π coverage in solid angle¹. It consists of an inner tracking detector surrounded by a thin superconducting solenoid providing a 2 T axial magnetic field, electromagnetic and hadronic calorimeters, and a muon spectrometer. The inner tracking detector covers the pseudorapidity range $|\eta| < 2.5$ and consists of silicon pixel, silicon microstrip, and transition radiation tracking detectors.

¹ ATLAS uses a right-handed coordinate system with its origin at the nominal interaction point (IP) in the centre of the detector and the z -axis along the beam pipe. The x -axis points from the IP to the centre of the LHC ring, and the y -axis points upwards. Cylindrical coordinates (r, ϕ) are used in the transverse plane, ϕ being the azimuthal angle around the z -axis. The pseudorapidity is defined in terms of the polar angle θ as $\eta = -\ln \tan(\theta/2)$. Angular distance is measured in units of $\Delta R \equiv \sqrt{(\Delta\eta)^2 + (\Delta\phi)^2}$.

The innermost layer, known as the insertable B-Layer [12, 13], was added in 2014 and provides high-resolution hits at small radius to improve the tracking performance. Lead/liquid-argon (LAr) sampling calorimeters provide electromagnetic (EM) energy measurements with high granularity. A hadronic (steel/scintillator-tile) calorimeter covers the central pseudorapidity range ($|\eta| < 1.7$). The endcap and forward regions are instrumented with LAr calorimeters for both the EM and hadronic energy measurements up to $|\eta| = 4.9$. The muon spectrometer surrounds the calorimeters and is based on three large air-core toroid superconducting magnets with eight coils each and bending power of 2.0 to 7.5 Tm. It includes a system of precision tracking chambers covering the region $|\eta| < 2.7$ and fast detectors for triggering in the range $|\eta| < 2.4$. A two-level trigger system was used to select events [14]. The first-level trigger is implemented in hardware and used a subset of the detector information to reduce the accepted rate to at most 100 kHz. This is followed by the software-based high-level trigger, which reduces the event rate to around 1 kHz.

3 Data and Simulation

3.1 Data sample and object definition

The analysis is performed with the 2015 and 2016 proton–proton collision data sample produced by the LHC at a centre-of-mass energy of $\sqrt{s} = 13$ TeV and collected by the ATLAS experiment, corresponding to an integrated luminosity of 36.1 fb^{-1} [15]. The data analysed were recorded during stable beam conditions and with all relevant ATLAS detector subsystems operational.

Electron candidates are reconstructed from energy deposits (clusters) in the electromagnetic calorimeter associated to reconstructed tracks in the inner detector. Candidates in the calorimetry transition region $1.37 < |\eta_{\text{cluster}}| < 1.52$ are excluded. Muon candidates are reconstructed from track segments in the layers of the muon spectrometer, and matched with tracks found in the inner detector. The final muon candidates are refit using the complete track information from both detector systems. Candidate jets are reconstructed from three-dimensional topological EM-scale energy clusters [16] in the calorimeter using the anti- k_t jet algorithm [17] with a radius parameter $R = 0.4$. The reconstructed jets are calibrated to the level of stable-particle jets by the application of a jet energy scale (JES) derived from simulation and *in situ* corrections based on 13 TeV data [18]. The missing transverse momentum, E_T^{miss} , is defined as the magnitude of the negative vector sum p_T of all reconstructed and calibrated physics objects in the event, with an extra term added to account for soft energy in the event that is not associated to any of the reconstructed objects [19]. This soft term is calculated from inner detector tracks matched to the primary vertex to make it more resilient to contamination from multiple pp collisions in the same or neighbouring bunch crossings (pileup).

3.2 Object and event selections

The event selection is designed to collect a sample of $t\bar{t}$ candidate events in the final state $\ell\nu bj j'\bar{b}$, where $\ell = e, \mu$, the jj' are the jets produced in the decay of the W boson to quarks, and at least one of the b -originated jets displays a semileptonic muon decay from a b -hadron. The goal is to select events where the lepton ℓ from the W boson and the b -originated jet with the muon from semileptonic decay come from the same top quark.

Events are required to pass either a single-electron or single-muon trigger. Multiple trigger types were used: the lowest-threshold triggers include isolation requirements to reduce the trigger rate, and had transverse momentum (p_T) thresholds of 20 GeV for muons and 24 GeV for electrons in 2015 data, or 26 GeV for both lepton types in 2016 data [20] [21]. These triggers were complemented by others with higher p_T thresholds and no isolation requirements to increase event acceptance. Events must have at least one reconstructed vertex, i.e. at least two tracks with $p_T > 0.4$ GeV consistent with the beam-collision region in the $x - y$ plane. If multiple vertices are reconstructed, the vertex with the largest sum of the squared transverse momenta of its associated tracks is taken as the primary vertex.

After trigger preselection, events are selected based on the presence of a candidate electron or muon from the decay of a W boson, called “primary” leptons. Electron candidates must pass a “tight” likelihood-based identification criterion [22], be matched to the corresponding trigger, have $p_T > 27$ GeV, $|\eta| < 2.47$ with the exclusion of $1.37 < |\eta| < 1.52$, longitudinal impact parameter $|z_0 \sin \theta| < 0.5$ mm and transverse impact parameter significance $|d_0/\sigma(d_0)| < 5$, where $\sigma(d_0)$ is the uncertainty in the transverse impact parameter. To reduce background from non-prompt electrons, photon conversions and hadrons, the prompt electrons must pass an isolation requirement based on the surrounding tracks and topological clusters in the calorimeter [22]. Muon candidates as primary leptons must pass a “medium” quality identification criterion [23], be matched to the corresponding trigger, have $p_T > 27$ GeV, $|\eta| < 2.5$, longitudinal impact parameters $|z_0 \sin \theta| < 0.5$ mm and transverse impact parameter significance $|d_0/\sigma(d_0)| < 3$. To reduce background from non-prompt muons and hadrons, muon candidates of this type must pass an isolation requirement based on the surrounding tracks and topological clusters in the calorimeter, and be separated by $\Delta R > 0.4$ from the nearest selected jet. If the nearest selected jet is within $\Delta R \leq 0.4$ of the muon and has less than three associated tracks, the muon is kept and the jet is removed from the jet list, to ensure high efficiency for muons undergoing significant energy loss in the calorimeter. Events with more than one candidate primary lepton with $p_T > 25$ GeV are vetoed, in order to reject events from the $t\bar{t}$ dileptonic decay channel.

Jet candidates are required to have $p_T > 25$ GeV and $|\eta| < 2.5$. A multivariate jet-vertex-tagger (JVT) is applied to suppress jets from pileup, requiring the JVT parameter to be greater than 0.59 for those jets with $p_T < 60$ GeV and $|\eta| < 2.4$ [24]. During jet reconstruction, no distinction is made between identified electrons and jet energy deposits. Therefore, if any of the jets lie within ΔR of 0.2 of a selected electron, the single closest jet is discarded in order to avoid double-counting of electrons as jets. After this, electrons which are within ΔR of 0.4 of a remaining jet are removed. Jets are identified as originating from a b quark (b -tagged) using two techniques, one based on the reconstruction of a displaced jet vertex (DV tagging) and the other based on the semileptonic decay of a b -hadron into a so-called “Soft muon” (SMT tagging). For the DV, multivariate techniques are used to combine information from the impact parameter of displaced tracks as well as topological properties of secondary and tertiary decay vertices reconstructed within the jet [25]. The algorithm is trained on simulated $t\bar{t}$ events to discriminate b -jets from a background consisting of light-flavour jets and c -jets. A selection corresponding to an efficiency of 77% for b -jets in $t\bar{t}$ events is employed. The SMT tagging is performed by requiring the presence of a muon candidate passing the “tight” quality identification criterion [23], $p_T > 8$ GeV and $|\eta| < 2.5$, with loose requirements on the impact parameter ($|d_0| < 3$ mm, $|z_0 \sin \theta| < 3$ mm) and within a distance $\Delta R < 0.4$ of a selected jet candidate. The definition of the muon object for the SMT tagging has been optimised by maximising the efficiency for muons originating from the semileptonic decays of b hadrons (selecting approximately 50% of b -jets containing a muon, which are in turn 20% of all b -jets produced in $t\bar{t}$ events), minimising the mis-identification rate (about 10^{-3} per light jet), and minimising the uncertainty on the measured top quark mass. If more than one muon passing the criteria above is found within a given jet, the muon with

the highest p_T is chosen. The background to SMT muons from heavy-flavour decays is mostly due to the decays of pions and kaons from light-flavour jets.

Events must have at least one SMT-tagged jet and one DV-tagged jet (which could be the same jet), among a total of at least four candidate jets with $p_T > 30$ GeV (with the exception of the SMT-tagged jet which may have a p_T as low as 25 GeV). If more than one SMT-tagged jet is found in the event, only the one with the highest p_T muon is considered. The SMT muon and the primary lepton must be separated by $\Delta R_{\ell,\mu} < 2$. Finally, the presence of at least one neutrino in the final state is inferred from the requirements that $E_T^{\text{miss}} > 30$ GeV and $E_T^{\text{miss}} + m_T(W) > 60$ GeV.² The selected sample is categorised as same-sign (SS) events or opposite-sign (OS) events according to the charge signs of the primary lepton and the soft muon. Opposite-sign events are enriched in direct $b \rightarrow \mu X$ decays, while same-sign events have a large contribution from sequential $b \rightarrow cX' \rightarrow \mu X''$, but both samples carry information on the mass of the parent top quark. The requirement that the SMT muon and the primary lepton must be separated by $\Delta R_{\ell,\mu} < 2$ enhances the fraction of events where both leptons come from the same top quark, in contrast to events where the two leptons originate from different top quarks. Finally, the invariant mass between the primary lepton and the soft muon ($m_{\ell\mu}$) is required to be between 15 and 80 GeV, as this is the region most sensitive to the top quark mass. This requirement also suppresses the Z -boson, J/ψ and Υ resonances.

The main backgrounds to candidate signal events come from the production of a single top quark, and from a W - or Z -boson in association with jets. A small background contribution arises from diboson (WW , WZ , ZZ) production. Events not containing real prompt leptons also contribute to the selected sample via the mis-identification of a jet or a photon as an electron, or the presence of non-prompt electrons or muons passing the prompt isolated lepton selection. This contribution is referred to as “multijet” background, and estimated in data following the matrix method described in Ref. [26].

3.3 Monte Carlo simulations

A number of Monte Carlo (MC) simulation samples are used to model the expected signal of top quark pairs and the background. The MC samples were processed either through the full ATLAS detector simulation [27] based on GEANT4 [28], or through a faster simulation making use of parametrised showers in the calorimeters [29]. Additional simulated pp collisions generated using PYTHIA-8.186 [30] with the MSTW2008 [31, 32] LO PDF set and the AUET2 [33] tune were overlaid to model the effects of both in- and out-of-time pileup. They are superimposed on the MC events, matching the luminosity profile of the recorded data. All simulated samples were processed through the same reconstruction algorithms and analysis chain as the data. Simulated MC events are corrected so that the object identification efficiencies, energy and momentum scale and resolution match those determined from data control samples. The modelling of SMT muons and their mis-identification is studied using control samples as well. The calibration of the mis-identification rate is performed using a sample of $W+1$ jet events, as in Ref. [34]. A data to simulation scale factor (SF) of 1.10 ± 0.14 is derived. The efficiency for the muon identification in jets is calibrated using muons from the decays of J/ψ and Z , and checked as a function of the surrounding track and calorimeter activities, and of the muon transverse impact parameter d_0 . The p_T of jets which contain a soft muon is corrected in the simulation with a factor of 0.967 ± 0.024 , to match the profile in data of the ratio of p_T between the SMT-tagged jet and the average non-SMT tagged jet.

² The $m_T(W) = \sqrt{2p_T^\ell E_T^{\text{miss}}(1 - \cos \Delta\phi)}$, where p_T^ℓ is the transverse momentum (energy) of the muon (electron) and $\Delta\phi$ is the azimuthal angle separation between the lepton and the direction of the missing transverse momentum.

The $t\bar{t}$ sample is generated using the *h_vq* program [35] in the POWHEG-Box V2 generator [36, 37] with the NNPDF3.0 parton distribution function (PDF) set [38] and the top quark mass set to 172.5 GeV. Additional samples with different top quark mass hypotheses were produced in the range of m_t between 165 and 180 GeV, with steps of 0.5 GeV between 170 and 175 GeV. The *h_vq* program uses on-shell matrix elements for next-to-leading (NLO) order in Quantum Chromodynamics (QCD) production of $t\bar{t}$ pairs. Off-shell effects and top-quark decays, including spin correlations, are introduced in an approximate way with Madspin [39]. Parton shower and hadronisation are modelled by PYTHIA 8.2 [30] using a dedicated A14- r_b setting as explained later in this section. Radiation in top quark decays is fully handled by the parton-shower generator, which implements matrix-element corrections with accuracy equivalent to the NLO level. The h_{damp} parameter, which controls the p_T of the first additional emission beyond the Born configuration, is set to 1.5 times the top quark mass of $m_t = 172.5$ GeV. The main effect of the h_{damp} setting is to regulate the high- p_T emission against which the $t\bar{t}$ system recoils. The ATLAS A14 [40] tune is based on LEP and Tevatron collider data and further uses a combination of ATLAS measurements from the 7 TeV collision data of underlying event, jet production, Z -boson production and top quark production to constrain the shower, multiple parton interactions and colour reconnection parameters. In addition, the STRINGZ:RFACB PYTHIA8 parameter (called henceforth r_b) of the fragmentation function was determined based on the b -quark fragmentation measured in e^+e^- collision data and extrapolated to proton–proton collisions, as described in Sec. 3.4. This setting is referred to as A14- r_b and is used in all MC samples using PYTHIA8 for the simulation of the parton shower.

The EVTGEN v1.2.0 [41] program is used to simulate the bottom and charm hadron decays. The production fractions and the branching ratios (BR) of the decay of b -hadrons and c -hadrons to muons are rescaled to the latest values from the Particle Data Group (PDG) [1], as detailed in Sec. 3.4. The simulated $t\bar{t}$ event sample is normalised to the top++2.0 [42] theoretical cross section of 832^{+46}_{-51} pb, calculated at next-to-next-to-leading order (NNLO) in QCD that includes resummation of next-to-next-to-leading logarithmic (NNLL) soft gluon terms [43–47].

Samples of W/Z +jets events and diboson production in association with jets, are simulated using the SHERPA 2.2.1 [48] generator. In the W/Z +jets samples, matrix elements are calculated for up to two partons at NLO and four partons at leading order (LO) using the COMIX [49] and OPENLOOPS matrix element generators and merged with the SHERPA parton shower [50], using the ME+PS@NLO prescription [51]. The CT10 PDF set is used in conjunction with dedicated parton shower tuning developed by the SHERPA authors. The normalisation of the W +jet background and the relative fractions of W boson associated with heavy flavour quark are extracted from data, taking advantage of the intrinsic W charge-asymmetry of the process [52]. The Z +jets contribution is estimated from MC simulation and checked in a data control sample. The diboson+jets samples are generated following the same approach but with up to one (ZZ) or zero (WW , WZ) additional partons at NLO and up to three additional partons at LO. They are normalised to their respective theoretical NLO cross sections calculated by the generator.

Samples of Wt and s -channel single top quark background events are generated with POWHEG-Box V1 and V2, respectively, with the CT10 PDF set. Overlaps between the $t\bar{t}$ and Wt final states are removed with the diagram removal prescription [53]. Electroweak t -channel single top quark events are generated using the POWHEG-Box V1 generator which uses the four-flavour scheme for the NLO matrix elements calculations together with the fixed four-flavour PDF set CT10f4. For this process, the top quarks are decayed using MadSpin [54], preserving all spin correlations. All single top quark samples are interfaced to PYTHIA 6.428 [55] with the Perugia 2012 [56] underlying-event tune. The EVTGEN v1.2.0 program is used to model properties of the bottom and charm hadron decays. The single top quark t - and s -channel samples are normalised to the approximate NNLO theoretical cross sections [57–59].

3.4 Modelling of heavy-quark fragmentation, hadron production and decays

The modelling of the momentum transfer between the b -quark and the b -hadron is an important aspect of this analysis. Monte Carlo event generators, such as the PYTHIA, HERWIG [60, 61] and SHERPA programs, describe this transition according to phenomenological models, namely the string and cluster models containing parameters which are tuned to data. PYTHIA8 allows the use of several parameterisations for the b -quark fragmentation function, while HERWIG7 and SHERPA use a non-parametric model which handles the complete parton shower evolution. The free parameters in those models are typically fit to measurements from e^+e^- colliders, and this analysis assumes that b -quark fragmentation properties at a reference q^2 scale are the same in e^+e^- and hadron collisions.

In this analysis, the Lund-Bowler parametrisation [62, 63] for PYTHIA8 is used. It is given by:

$$f(z) = \frac{1}{z^{1+br_b m_b^2}} (1-z)^a \exp(-bm_T^2/z), \quad (1)$$

where a , b and r_b are the function parameters, m_b is the b -quark mass, m_T the b -hadron transverse mass and z is the fraction of the longitudinal energy of the b -hadron with respect to the b -quark, in the light cone reference frame. The fragmentation function is defined at the hadronisation scale and it is evolved by the parton shower to the process scale through DGLAP evolution equations. In PYTHIA8, the values of a and b have been fitted to data sensitive to light quark fragmentation [64], such as charged multiplicities, event shapes and scaled momentum distributions. They are then assumed to be universal between light and heavy quarks, while the r_b parameter is specific to b -quark fragmentation. To improve the description of b -quark fragmentation, following Refs. [65–68], a fit is performed for the r_b parameter in PYTHIA8 using data from ALEPH, DELPHI and OPAL at the LEP collider, and from the SLD experiment at the SLC collider [69–72]. The distribution of $x_B = 2p_B \cdot p_Z / m_Z^2$ from semileptonically decaying b -hadrons in $e^+e^- \rightarrow Z \rightarrow b\bar{b}$ events is used, where p_B and p_Z are the four-momenta of the b -hadron and the Z , respectively. In the Z rest frame, m_Z is twice the beam energy and therefore $x_B = 2E_B/m_Z$, where E_B is the energy of the b -hadron. The fit is performed using PROFESSOR v2.2 [73] for the minimisation, and Rivet v2.5.4 [74] for the implementation of the measurements and gives the result $r_B = 1.05 \pm 0.02$.

The production fractions of weakly decaying b - and c -hadrons described in POWHEG+PYTHIA8 MC simulation with EVTGEN are rescaled to those from the Heavy Flavour Averaging Group (HFLAV) [75] as reported in the PDG [1] and in Ref. [76]. The production fraction values and corresponding scale factors for POWHEG+PYTHIA8 simulations are shown in Table 1. Scale factors are applied to each heavy-quark hadron present in a MC simulated event, with the overall event weight given by the product of all heavy-quark hadrons in that event.

The branching ratios of the b - and c -hadron decays that contain a μ are also adjusted to match those as measured by previous experiments [1]. Central values and relative scale factors, along with the corresponding uncertainties, are shown in Table 2. The $b \rightarrow \bar{c} \rightarrow \mu$ branching ratio was determined averaging the direct measurement from DELPHI [77] and the predicted values computed by the LEP Electroweak Heavy Flavour Working Group [78]. The latter prediction was based on flavour-specific $B \rightarrow D$ and $B \rightarrow \Lambda_c^+$ rates measured at CLEO [79–81] in combination with the $B \rightarrow DD(X)$ rates measured in ALEPH [82] to extract the probabilities of producing the different c -hadrons from the initial b -hadrons decays. The c -hadron semileptonic branching fractions were also used in the prediction. The $c \rightarrow \mu$ scale factor is applied only to the semileptonic decays of c -hadrons to muons when the c -hadrons do not come from a cascade b -hadron decay.

Table 1: The production fraction values for b -hadrons and c -hadrons in the PDG and POWHEG+PYTHIA8. The values under the PDG column are derived from Ref. [1] and [76]. The same scale factors are applied to the charge-conjugate hadrons.

Hadron	PDG (%)	POWHEG+PYTHIA8	Scale Factor
B^0	0.404 ± 0.006	0.429	0.941
B^+	0.404 ± 0.006	0.429	0.942
B_s^0	0.103 ± 0.005	0.095	1.088
b -baryon	0.088 ± 0.012	0.047	1.874
D^+	0.226 ± 0.008	0.290	0.780
D^0	0.564 ± 0.015	0.553	1.020
D_s^0	0.080 ± 0.005	0.093	0.857
c -baryon	0.109 ± 0.009	0.038	2.898

Table 2: Hadron to μ branching ratios and scale factors applied to POWHEG+PYTHIA8. The values under the PDG column are derived from Ref. [1] and [76]. The $c \rightarrow \mu$ scale factor is applied only to the semileptonic decays of c -hadrons to muons when the c -hadrons do not come from a cascade b -hadron decay. The same scale factors are applied to the charge conjugate hadrons.

Hadron	PDG	POWHEG+PYTHIA8	Scale Factor
$b \rightarrow \mu$	$0.1095^{+0.0029}_{-0.0025}$	0.106	1.032
$b \rightarrow \tau$	0.0042 ± 0.0004	0.0064	0.661
$b \rightarrow c \rightarrow \mu$	0.0802 ± 0.0019	0.085	0.946
$b \rightarrow \bar{c} \rightarrow \mu$	$0.016^{+0.003}_{-0.003}$	0.018	0.888
$c \rightarrow \mu$	0.082 ± 0.005	0.084	0.976

4 Analysis

4.1 Event yields and sample composition

The number of observed candidate events and the predicted signal and background is shown in Table 3, for both the OS and SS regions. The sample consists of about 90% top quark pairs, which includes cases where the soft muon is erroneously chosen from a $t\bar{t}$ dilepton decay, whereby a muon from the prompt W decay is found near a jet or radiates a near-collinear photon mimicking a soft muon tag, and cases where the soft muon does not originate from a b decay. The contributions from single top quark, W - or Z -boson in association with jets, and from multijet background are visible. The Z +jets background gives a small contribution near the peak of the $m_{\ell\mu}$ distribution, but becomes important for $m_{\ell\mu}$ close to the Z -boson mass peak.

Of the selected $t\bar{t}$ events in the OS class, in 83% of the cases the primary lepton and the soft muon belong to the decay of the same top quark, while in 10% of the events the two originate from different top quarks. Much of the purity obtained in this sample is due to the topological requirement $\Delta R_{\ell,\mu} < 2$, which is very effective in selecting preferentially the same-top decays. For the remaining cases, 7%, the soft muon does not originate from any of the two nominal b -quarks from the top pair decay. In the SS class, the above

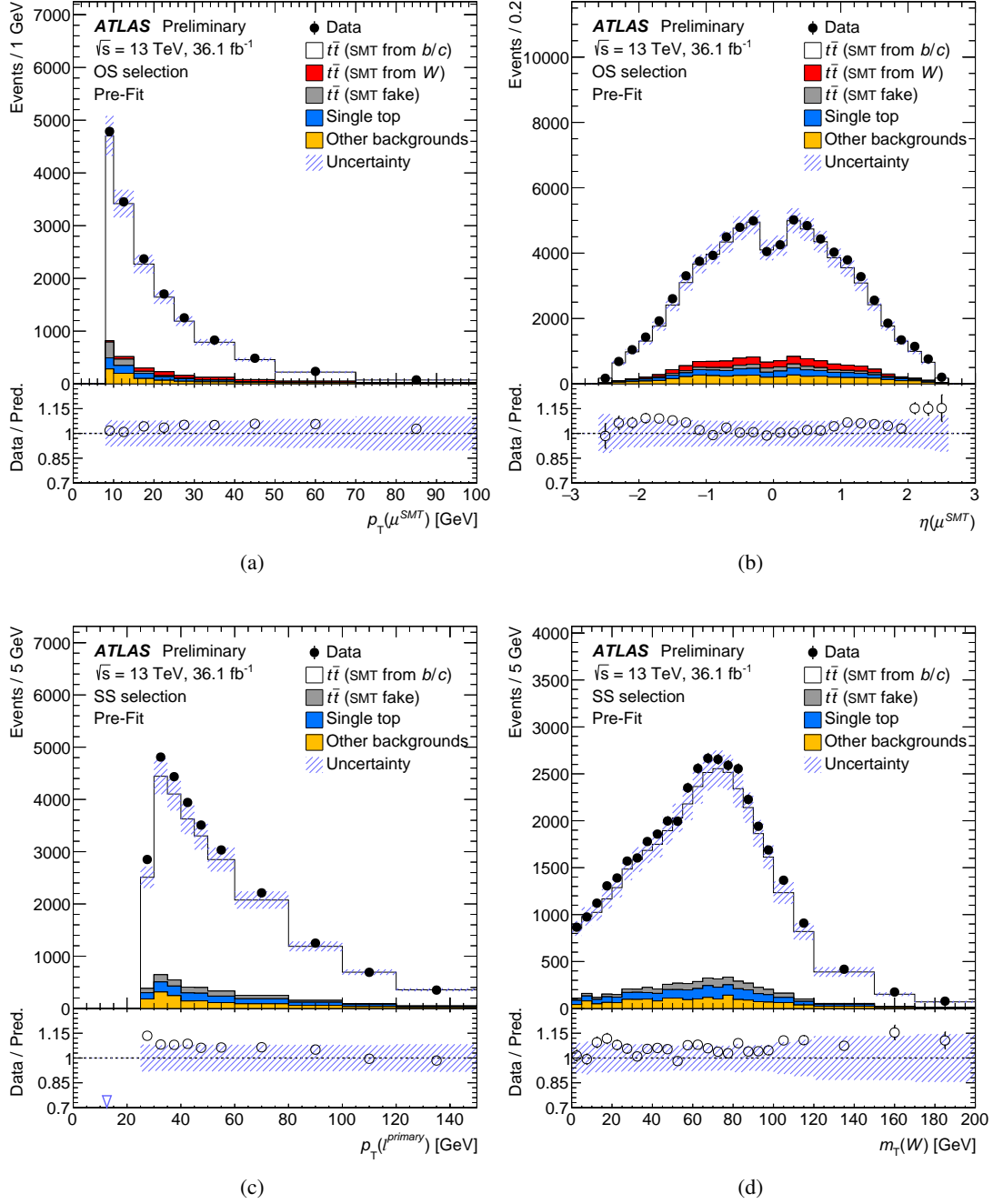


Figure 1: Comparison of data and prediction in the OS (top) and SS (bottom) samples, for the soft muon p_T (a), soft muon η (b), primary lepton p_T (c) and the W boson transverse mass (d). The prediction reports the expected event contribution for the signal and backgrounds. The uncertainty band includes statistical and systematic uncertainties. The same-sign (SS) or opposite-sign (OS) refers to the charge signs of the primary lepton and the soft muon.

fractions are 57%, 41% and 2%, respectively. The higher rate of non- b originated soft muons in OS events is due to the charm from the $W \rightarrow cs$ in the top-quark decay chain.

Table 3: Events yields with $m_{\ell\mu}$ between 15 and 80 GeV, separately for OS and SS regions. Uncertainties shown include statistical and systematic contributions.

Process	Yield (OS)		Yield (SS)	
$t\bar{t}$ (SMT from b - or c -hadron)	56 000	± 4000	34 800	± 2800
$t\bar{t}$ (SMT from $W \rightarrow \mu\nu$)	2190	± 320	4.9	± 3.6
$t\bar{t}$ (SMT fake)	1490	± 210	1240	± 170
Single top t -chan	770	± 70	490	± 40
Single top s -chan	63	± 6	49	± 4
Single top Wt	1840	± 140	1260	± 100
W +jets	1600	± 400	1080	± 240
Z +light jets	210	± 80	15	± 6
Z +HF jets	550	± 170	310	± 100
Diboson	17.2	± 2.9	6.3	± 1.4
Multi-jet	530	± 140	480	± 130
Total Expected	65 000	± 5000	39 800	± 3000
Data	66 891		42 087	

To understand the nature of the sample composition in the OS and SS regions, the expected $t\bar{t}$ events can be further split into components involving direct and sequential decays, and decays not belonging to the b from the $t \rightarrow Wb$ path, as shown in Table 4.

Table 4: Fraction of MC-simulated $t\bar{t}$ events split into components of direct and sequential decays, and decays not belonging to the b from the $t \rightarrow Wb$ path, separately for the opposite-sign and same-sign event selections. The capital letters B and D indicate b and c hadrons of either charge. Only MC events with two real muons are included.

	OS [%]	SS [%]
Processes involving a μ from a t or \bar{t}		
$t \rightarrow B \rightarrow \mu$	73.6	51.2
$t \rightarrow B \rightarrow D \rightarrow \mu$	16.7	44.2
$t \rightarrow B \rightarrow \tau \rightarrow \mu$	2.0	1.3
$t \rightarrow B \rightarrow D \rightarrow \tau \rightarrow \mu$	0.8	0.8
Processes involving a μ not from a t or \bar{t}		
$B \rightarrow \mu$	0.6	0.9
$D \rightarrow \mu$	5.8	1.4
$\tau \rightarrow \mu$	0.5	0.1

The data are compared to the sum of the predicted signal and backgrounds in Figure 1, for an illustrative selection of kinematic distributions of the candidate events: the $p_T(\mu^{\text{SMT}})$, $\eta(\mu^{\text{SMT}})$ for the OS selection and $p_T(\ell^{\text{primary}})$, $m_T(W)$ for the SS selection. The consistency of the data and MC predictions has been studied using a χ^2 test involving the full correlation matrix, and for all distributions the agreement is at the level of 2 standard deviations or better.

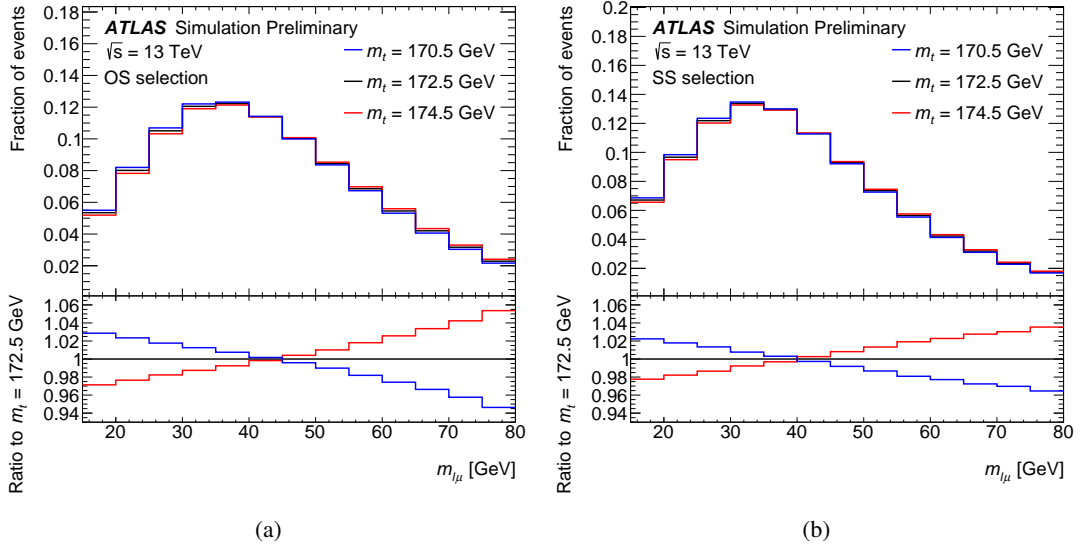


Figure 2: Sensitivity of the $m_{\ell\mu}$ distribution to different input top quark mass from simulated events, separately for the OS and SS samples.

4.2 Extraction of the top quark mass

The distribution of the invariant mass between the primary lepton and the soft muon, $m_{\ell\mu}$ is used to determine the mass of the parent top quark. A binned-template profile likelihood fit is performed, with a Poisson likelihood model and systematic uncertainties included as Gaussian-constrained nuisance parameters. Only the range of $m_{\ell\mu}$ between 15 and 80 GeV is considered in the fit, since the tail of the $m_{\ell\mu}$ distribution is more sensitive to $t\bar{t}$ modelling uncertainties and higher order corrections, and to the Z +jets background. The fit is performed simultaneously for the OS and SS charge-combination samples, and Figure 2 shows the sensitivity of each of these distributions to variations of the top quark mass, as well as the binning used by the templates.

The fit uses template histograms simulated as the nominal $t\bar{t}$ sample but with different values for the input top quark mass. Samples were generated with 12 different top quark mass values, ranging between 165.0 GeV and 180.0 GeV in variable mass-value steps of up to 0.5 around 172.5 GeV. The templates from the different mass samples are interpolated with piece-wise linear functions built bin-by-bin. To improve the stability of the method, the templates are smoothed assuming a linear dependence of the fraction of total events in each bin on m_t . A maximum likelihood fit is performed with three free parameters: m_t , which controls the shape of the $m_{\ell\mu}$ distribution for $t\bar{t}$ events, and the normalisation factors for $t\bar{t}$ events in the OS and SS samples. The uncertainty due to the limited number of simulated events, and due to statistical fluctuations in the background estimates based on control samples, is evaluated by defining a new source of systematic uncertainty for each bin of the prediction, which modifies the bin content by its statistical uncertainty. A pruning procedure is applied to reduce the number of insignificant systematic uncertainties affecting the prediction of each of the signal and background processes, but does not affect significantly the estimated uncertainties.

The top quark mass determination from the fit is found to be linear and unbiased with respect to the input top quark mass hypothesis by means of pseudo experiments, and its uncertainty from the likelihood ratio is

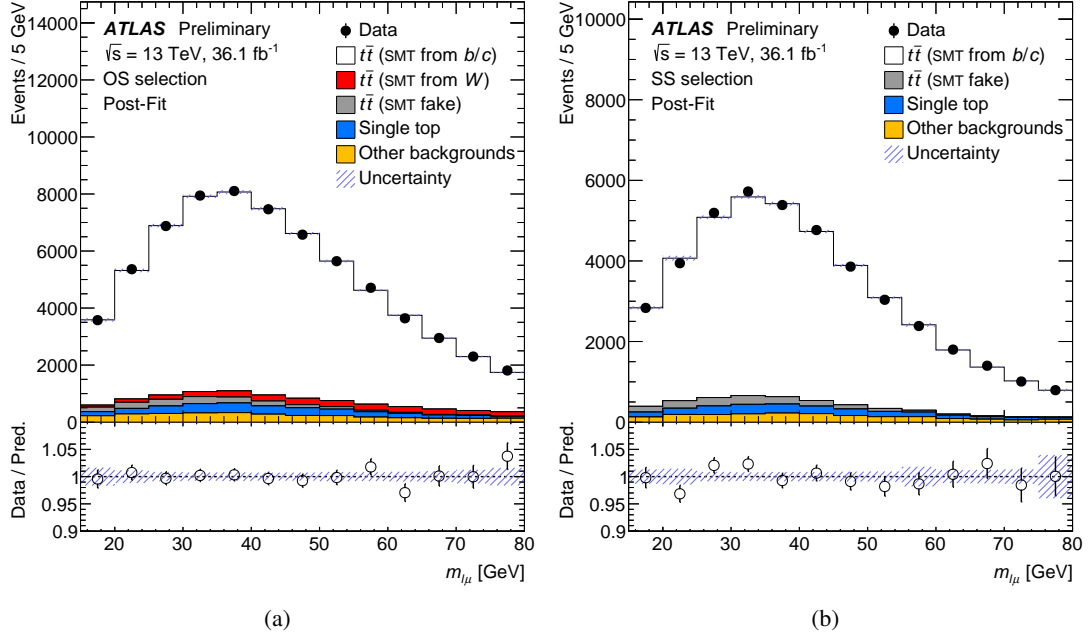


Figure 3: Post-fit $m_{\ell\mu}$ distributions in the OS sample (a) and in the SS sample (b). The prediction reports the event contribution for the signal and backgrounds. The uncertainty band includes statistical and systematic uncertainties. The same-sign (SS) or opposite-sign (OS) refers to the charge signs of the primary lepton and the soft muon

also checked to ensure it reports the correct statistical coverage. The fit method and the event selection were optimised to minimise the total uncertainty on m_t in a “blinded” approach, that is using pseudo-data and data without knowledge of the best-fit top quark mass. The fit gives:

$$m_t = 174.48 \pm 0.40 \text{ (stat)} \pm 0.67 \text{ (syst)} \text{ GeV}, \quad (2)$$

corresponding to a total uncertainty of ± 0.78 GeV. Figure 3 shows the post-fit $m_{\ell\mu}$ distributions in the OS and SS samples. The pulls and constraints of the nuisance parameters in the combined fit to data are shown in Figure 4 (a), and the likelihood scan with the best-fit top quark mass value in Figure 4 (b). The systematic uncertainties are discussed in Section 4.3.

A goodness-of-fit test is performed using the saturated model technique [83] and returns a probability of 56%. Checks were performed by fitting separately the OS and SS regions, the electron and muon channels, different W lepton charge and different configurations of b -tagging and event selection, and were found to give consistent results. Checks included also the extraction of the top quark mass with alternative statistical methods, namely using analytic functions for $m_{\ell\mu}$ with a parametric dependence on the top quark mass, only using the mean value of the $m_{\ell\mu}$ distribution, and using a binned-template likelihood fit without including systematic uncertainties as nuisance parameters. In particular the inclusion of systematic uncertainties as nuisance parameters in the fit reduces the total uncertainty by 4.9%, in line with reasonable constraints from the fit.

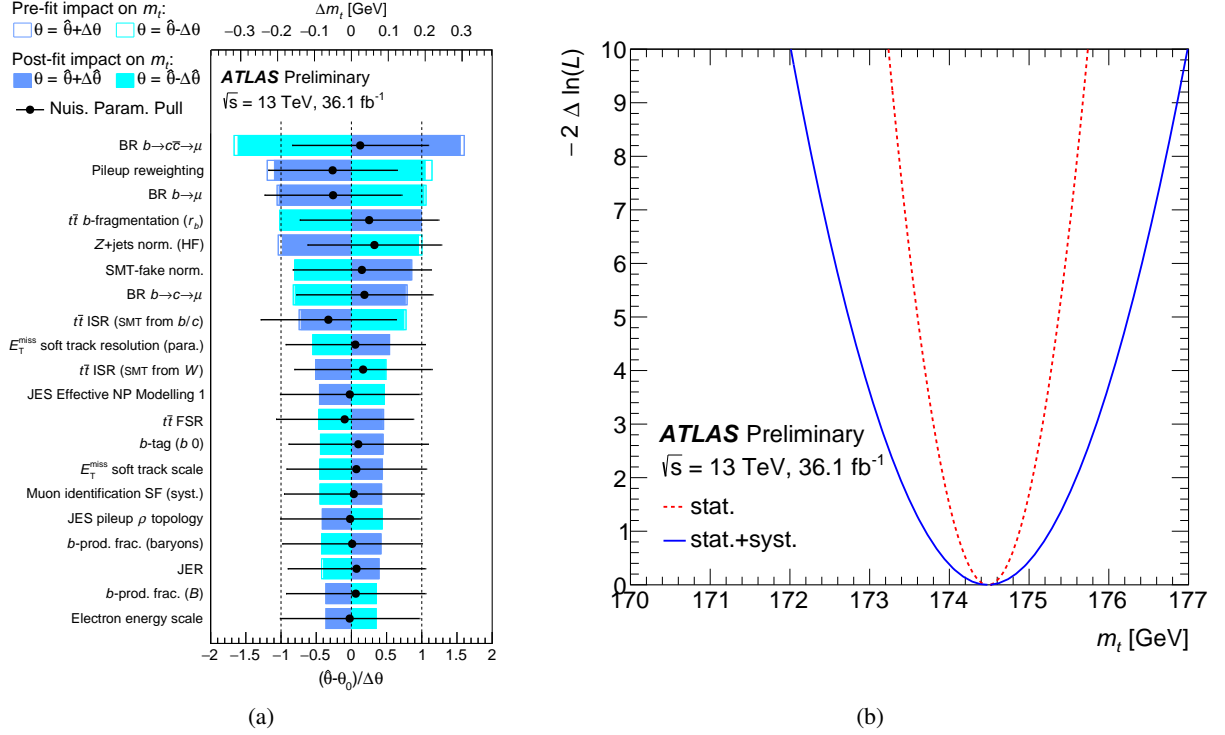


Figure 4: (a): Ranking of the main systematic uncertainties, showing the pulls and the impact of constraining the systematic uncertainties, from the combined OS and SS binned template profile-likelihood fit to data. (b): Likelihood scan, showing the best-fit value and the statistical and total uncertainty profiles.

4.3 Systematic uncertainties

Many sources of systematic uncertainties are considered, corresponding to a total of 146 individual variations. The uncertainty in the combined 2015-2016 integrated luminosity is 2.1% [15], obtained using the LUCID-2 detector [84] for the primary luminosity measurements. The distribution of the average number of interactions per bunch crossing in MC samples are reweighted to match the conditions in data, and a corresponding uncertainty is evaluated according to the uncertainty on the average number of interactions per bunch crossing [15]. The uncertainty due to the limited statistics of the simulated samples is considered both for the impact on the fit calibration, and for the uncertainty on the backgrounds which are estimated with MC samples.

Uncertainties associated with leptons arise from the trigger, reconstruction, identification, and isolation requirements, as well as the lepton momentum scale and resolution. The reconstruction, identification and isolation efficiency for electrons and muons, as well as the efficiency of the trigger, differ slightly between data and simulation and are compensated for by dedicated scale factors. Efficiency SFs are derived using data and simulated samples of $Z \rightarrow \ell^+ \ell^-$ ($\ell = e, \mu$), and are applied to the simulation to correct for differences. The uncertainties on these corrections are propagated throughout the analysis. The total uncertainty on efficiency SFs, for the high- p_T leptons, is $< 0.5\%$ for muons across the entire p_T spectrum [23] and for electrons with $p_T > 30$ GeV, while it exceeds 1% for lower p_T electrons [22]. Additional sources of uncertainty originate from the uncertainty on the corrections applied to adjust the lepton momentum scale and resolution in the simulation to match those in data. They are measured using reconstructed $Z \rightarrow \ell^+ \ell^-$ and $J/\psi \rightarrow \ell^+ \ell^-$ dilepton invariant mass distributions, as well as the measured

E/p in $W \rightarrow e\nu$ events, where E and p are the electron energy and momentum, as determined by the calorimeter and the inner detector respectively. To evaluate the effect of momentum scale uncertainties, the event selection is repeated with the lepton momentum varied by $\pm 1\sigma$. For the momentum resolution uncertainties the event selection is redone with the lepton momentum smeared. A systematic uncertainty due to the charge mis-identification for electrons has been evaluated as outlined in Ref. [22]. Scale factors correcting for the differences in electron charge mis-identification rates between data and simulation have been computed using $Z \rightarrow e^+e^-$ events.

The relative uncertainty on the normalisation of the soft muon component of $t\bar{t}$ events which arises from light hadron decays and detector background (“Soft muon fake modelling”) is evaluated using a control sample of $W+1$ jet events simulated with SHERPA, and is estimated to be 13%. An additional uncertainty is derived from the difference in shape and normalisation of the $m_{\ell\mu}$ distribution of SMT mistags between simulations of $t\bar{t}$ with POWEG+PYTHIA8 and SHERPA.

Uncertainties associated with jets arise from the efficiency of jet reconstruction and identification based on the JVT variable, as well as the jet energy scale (JES) and resolution (JER). Although the observable $m_{\ell\mu}$ does not involve jets, the various jet uncertainties impact the analysis through the event selection. The JES and its uncertainty were derived by combining information from test-beam data, LHC collision data and simulation [18]. The JES uncertainty is about 5.5% for jets with $p_T = 25$ GeV and quickly decreasing with increasing jet p_T . It is below 1.5% for central jets with p_T in the range of $\simeq 100$ GeV–1.5 TeV. The magnitude of the JER uncertainty variation is parametrised in jet p_T and η [85], and the uncertainty is propagated by smearing the jet p_T in the simulation. The uncertainty on the efficiency to pass the JVT requirement is evaluated by varying the scale factors within their uncertainties [24].

The E_T^{miss} reconstruction is affected by uncertainties associated with leptons and jet energy scales and resolutions, which are appropriately propagated to the E_T^{miss} calculation. Additional small uncertainties associated with the modelling of the underlying event, in particular its impact on the p_T scale and resolution of unclustered energy, are also taken into account [19].

The efficiencies of DV tagging in simulated samples are corrected to match efficiencies in data. Correction scale factors are derived for jets originating from b , c and light quarks separately in dedicated calibration analyses [25, 86, 87]. For jets originating from b - and c -quarks, SFs are derived as a function of p_T , whereas the light-jet efficiency is scaled by p_T - and η -dependent factors. Uncertainties on the correction scale factors are estimated by varying each source of uncertainty up and down by one standard deviation and are taken as uncorrelated between b -jets, c -jets, and light-jets. An additional set of MC-to-MC correction factors are introduced to account for the different parton shower and hadronisation model used in the calibration samples with respect to those used in this analysis. Furthermore, the efficiency of tagging the hadronic decays of τ -leptons in simulation is treated in the same way as the efficiency of tagging c -jets, and a specific uncertainty is considered for this simplified approach. Two additional uncertainties are included due to the extrapolation of SFs for jets with p_T beyond the kinematic reach of the data calibration samples. The same SFs are verified to also be applicable to jets containing soft muons. An additional check was performed by changing the event selection such that there is always a DV tagged jet other than the SMT tagged jet in the event, and the measured top quark mass is consistent with the value measured using the nominal event selection.

Uncertainties on $t\bar{t}$ signal modelling include all sources that affect the kinematics of the lepton from the W -boson decay and the kinematics of the b -hadron giving rise to the soft muon, but also the fraction of events from different soft-muon flavour components (from b -hadrons, c -hadrons, light jet and W -boson). The $t\bar{t}$ inclusive cross-section uncertainty does not affect the measurement, since no information is extracted

from the total number of selected events after background subtraction. Uncertainties due to the b -hadron production fractions and the BRs of the inclusive decays of b - and c -hadrons into muons are derived from the uncertainties on the rescaling procedure, described in Sec. 3.4 and shown in Tables 1 and 2. Those uncertainties are propagated throughout the analysis. In addition, a check was performed to verify that the impact on $m_{\ell\mu}$ of the mass of the D mesons involved in $b \rightarrow c\mu + X$ transitions was within the uncertainty assigned to $b \rightarrow \mu$ inclusive BRs. For this purpose, the exclusive decays $B^0 \rightarrow D^-\mu\nu$, $B^0 \rightarrow D^{*-}(2010)^-\mu\nu$, $B^+ \rightarrow \overline{D}^0\mu\nu$, $B^+ \rightarrow \overline{D}^{*0}(2007)^0\mu\nu$ and their charge conjugates were considered. For each of these decays, a kinematic phase space similar to that of the main selection was applied to the events and the impact on $m_{\ell\mu}$ was found significantly smaller than the effect of varying only the BR of the inclusive $b \rightarrow \mu$ decays.

Uncertainties due to the choice of NLO matching scheme in the $t\bar{t}$ MC generator are estimated by comparing a sample generated with POWHEG+PYTHIA8 with a sample generated with MADGRAPH5_aMC@NLO+PYTHIA8 (referred to hereafter as aMC@NLO+PYTHIA8). The aMC@NLO matching requires specific settings of the PYTHIA8 shower to retain the NLO accuracy, where the matrix-element corrections are switched off for both initial-state radiation and the global-recoil settings are used for final-state radiation emissions, and these settings are different from the nominal POWHEG+PYTHIA8. In order to have a coherent comparison, an alternative POWHEG+PYTHIA8 sample was generated with the same PYTHIA8 configuration as that used to shower aMC@NLO events. Additionally, since aMC@NLO+PYTHIA8 is known to describe poorly the distribution of the boost of the $t\bar{t}$ system ($p_T^{t\bar{t}}$) [88], the $p_T^{t\bar{t}}$ in aMC@NLO+PYTHIA8 is re-weighted to that of the POWHEG+PYTHIA8 sample. The full difference between the top quark mass obtained with the two samples is considered as the positive and negative uncertainty due to the NLO matching.

The modelling of the underlying event and of colour reconnection (CR) can affect the amount of radiation emitted from the b -quark, as well as modify the kinematic distribution of the b -hadron. An underlying event uncertainty is estimated with the corresponding eigentunes of the A14 PYTHIA8 tune. Variations of colour reconnection parameters are also provided by the A14 eigentunes, determined from measurements of the underlying event in jet production. Samples have been generated where the colour reconnection strength in the Pythia8 default model is set to its maximum value (all hadrons are reconnected) and are compared to a setting with the colour reconnection switched off. To account for the possibility of colour reconnection also affecting the top quark decay products, a comparison with the “Early Resonance Decay” (ERD) model has been performed [89]. In this model the top quarks and W bosons are allowed to decay before CR takes place, so the top quark decay products directly participate in CR. The impact on the measured top quark mass is found to be negligible.

The systematic uncertainty due to the choice of PDFs has been evaluated using the PDF4LHC15 error set applied to the nominal $t\bar{t}$ MC settings, and is performed by means of event re-weighting for 30 PDF replicas. The m_t value is extracted for each of the 30 cases, and the total systematic uncertainty due to this effect is computed as the sum in quadrature of the single variations.

The uncertainty on the modelling of initial-state radiation (ISR) is estimated by variations of the scales in POWHEG+PYTHIA8. A sample with increased radiation is obtained by multiplying the renormalisation and factorisation scale by a factor of 0.5, doubling the h_{damp} parameter and using a larger α_S^{ISR} value corresponding to the PYTHIA8 A14 VAR3cUP variation [90]. The sample with decreased radiation has the renormalisation and factorisation scales increased by a factor of 2.0 together with a lower α_S^{ISR} value, corresponding to the VAR3cDW variation of PYTHIA8 A14.

Parton shower and hadronisation uncertainties include several components. An alternative simulation of the $t\bar{t}$ sample has been considered whereby the POWHEG-Box generator has been matched to the HERWIG7.1.3

generator for the modelling of the parton shower and hadronisation. The HERWIG7.1.3 generator release includes several improvements in the shower description for heavy-quark fragmentation, together with a new tune to e^+e^- data. The angular-ordered shower algorithm is used, as it better describes both the shower evolution in the 7 TeV ATLAS measurement of jet shapes in $t\bar{t}$ events [91], and the x_B distribution of LEP data, although it does not describe the x_B spectrum of LEP data as well as PYTHIA8. The HERWIG7.1.3-based sample, when compared to the nominal $t\bar{t}$ simulation used in the fit, allows the effect of changes in the shower algorithm to be assessed, and therefore initial- and final-state emissions, using different but coherent models of hadronisation, underlying event and colour reconnection. The full difference between the top quark mass obtained with the two samples of POWHEG showered with PYTHIA8 A14- r_b and HERWIG7.1.3 is considered as the positive and negative uncertainty variation due to the parton shower and hadronisation modelling. Additional samples were produced varying the value of r_b within its uncertainty of ± 0.02 , and the impact on the measured top quark mass is added as a systematic uncertainty.

The uncertainty due to the final state radiation (FSR) renormalisation and factorisation scales on the evolution of the fragmentation function to the process energies was evaluated by generating alternative event samples with the scales varied up and down by factors of $\sqrt{2}$ [92], while keeping the fragmentation function at the LEP scale fixed, and the resulting impact on the top quark mass is added as a systematic uncertainty.

Numerous sources of uncertainties are considered for the normalisation and shape of the background contributions. For the $t\bar{t}$ dilepton component, uncertainties due to the modelling of the ISR, to the choice of NLO matching and to the parton shower and hadronisation model are estimated as done for the nominal $t\bar{t}$ sample. An uncertainty of $+5\%/ -4\%$ is applied to the total cross-section for single-top quark production [57–59]. An additional uncertainty on initial and final-state radiation is evaluated in a manner similar to that used for $t\bar{t}$. The uncertainty on the interference between Wt and $t\bar{t}$ production at NLO is assessed by comparing the default “diagram removal” scheme to an alternative “diagram subtraction” scheme [53]. The uncertainty due to the choice of the event generator for the t -channel is evaluated with a comparison to a sample simulated with aMC@NLO, and the uncertainty due to the parton shower and hadronisation models for the t and Wt channels is derived comparing with samples showered with HERWIG. An uncertainty of 30% is applied on the Z +jets background normalisation, both for its light-flavour-jet and heavy-flavour-jet ($Z+c\bar{c}$ and $Z+b\bar{b}$) components. The uncertainty is derived in simulation and validated in a control region around the Z -boson mass peak, where the normalisations of the Z +light-jet and Z +heavy-flavour-jet are simultaneously extracted with a combined fit and are found in agreement with the theoretical expectation of Z +jets. The uncertainty on the normalisation and on the flavour composition of W +jets is assessed in data control regions. The total normalisation and flavour fraction uncertainty is of about 22% for the $Wb(b)$ and Wcc , approximately 45% for Wc , and about 23% for W +light. For the multijet background, a 30% systematic uncertainty is assigned to the predicted yields, based on comparisons with data yields in control regions similar to the signal region but enriched in events coming from the multijet background; the e +jet and μ +jet events are treated as uncorrelated. The impact on the measured top quark mass from the statistical uncertainty on the shape of the $m_{\ell\mu}$ distribution for the multijet background is also evaluated. For the small diboson background, a 50% normalisation uncertainty is assigned and includes uncertainties on the inclusive cross-section and additional jet production [93]. Table 5 summarises the impact on m_t of the main sources of systematic uncertainties. Multiple sources shown in Fig. 4 are grouped together in this Table. The statistical uncertainties on m_t due to the limited number of simulated signal and background events, and the size of the data control sample used in the determination of the multijet background, are also reported. Each systematic uncertainty is accompanied by an estimate of its statistical precision.

Table 5: Impact of main sources of uncertainty on m_t . The last column shows the statistical uncertainty on each of the top quark mass uncertainties.

Source	Unc. on m_t [GeV]	Stat. precision [GeV]
Data statistics	0.40	
Signal and background model statistics	0.16	
Monte Carlo generator	0.04	± 0.07
Parton shower and hadronisation	0.07	± 0.07
Initial-state QCD radiation	0.17	± 0.07
Parton shower α_S^{FSR}	0.09	± 0.04
b -quark fragmentation	0.19	± 0.02
HF-hadron production fractions	0.11	± 0.01
HF-hadron decay modelling	0.39	± 0.01
Underlying event	< 0.01	± 0.02
Colour reconnection	< 0.01	± 0.02
Choice of PDFs	0.06	± 0.01
W/Z +jets modelling	0.17	± 0.01
Single top modelling	0.01	± 0.01
Fake lepton modelling ($t \rightarrow W \rightarrow \ell$)	0.06	± 0.02
Soft muon fake modelling	0.15	± 0.03
Jet energy scale	0.12	± 0.02
Soft muon jet p_T calibration	< 0.01	± 0.01
Jet energy resolution	0.07	± 0.05
Jet vertex tagger	< 0.01	± 0.01
b -tagging	0.10	± 0.01
Leptons	0.12	± 0.00
Missing transverse momentum modelling	0.15	± 0.01
Pile-up	0.20	± 0.05
Luminosity	< 0.01	± 0.01
Total systematic uncertainty	0.67	± 0.04
Total uncertainty	0.78	± 0.03

5 Conclusions

A direct measurement of the top quark mass has been performed using a technique that exploits a partial, leptonic-only, invariant mass reconstruction of the top quark decay products. The analysis, based on data corresponding to an integrated luminosity of 36.1 fb^{-1} of $\sqrt{s} = 13 \text{ TeV}$ pp collisions provided by the Large Hadron Collider and recorded by the ATLAS detector, uses as observable the invariant mass $m_{\ell\mu}$ between the lepton ℓ (with $\ell = e, \mu$) from the W -boson decay and the muon μ from a semileptonic decay of a b -hadron. A binned-template profile likelihood fit to the $m_{\ell\mu}$ distribution is performed to determine the most probable top quark mass value. The result, $m_t = 174.48 \pm 0.40 \text{ (stat)} \pm 0.67 \text{ (syst)} \text{ GeV}$, corresponds to the most precise single measurement to date of the top quark mass from the direct reconstruction of its decay products by the ATLAS Collaboration. The measurement is also significantly more precise than those with similar techniques performed before [6, 7]. The result is consistent at the level of about 2.2 standard deviations with the current ATLAS combination of top quark mass measurements from the reconstruction of the top quark decay [8]. A similar level of consistency is found with the equivalent combination at CMS [9], while the agreement with the latest Tevatron combination [10] is good. The main sources of systematic uncertainty are due to the modelling of the top quark pair production and of the b fragmentation and decay, with uncertainties from pileup and backgrounds also noticeable. On the other hand, the uncertainty due to the calibration of the jet energies is sub-dominant, which is advantageous in future combinations of this result with those from the standard reconstruction of the top quark decay products.

References

- [1] M. Tanabashi et al., *Review of Particle Physics*, [Phys. Rev. D **98** \(3 2018\) 030001](#) (cit. on pp. 2, 6–8).
- [2] G. Degrandi et al., *Higgs mass and vacuum stability in the Standard Model at NNLO*, [JHEP **2012** \(2012\) 98](#), arXiv: [1205.6497 \[hep-ph\]](#) (cit. on p. 2).
- [3] S. Alekhin, A. Djouadi and S. Moch, *The top quark and Higgs boson masses and the stability of the electroweak vacuum*, [Phys. Lett. B **716** \(2012\) 214](#), arXiv: [1207.0980 \[hep-ph\]](#) (cit. on p. 2).
- [4] P. Nason, *The Top Mass in Hadronic Collisions*, 2019, arXiv: [1712.02796 \[hep-ph\]](#) (cit. on p. 2).
- [5] G. Corcella, *The top-quark mass: challenges in definition and determination*, *Front. in Phys.* **7** (2019) 54, arXiv: [1903.06574 \[hep-ph\]](#) (cit. on p. 2).
- [6] T. Aaltonen et al., *Measurement of the Top Quark Mass Using the Invariant Mass of Lepton Pairs in Soft Muon b -tagged Events*, [Phys. Rev. D **80** \(2009\) 051104](#), arXiv: [0906.5371 \[hep-ex\]](#) (cit. on pp. 2, 18).
- [7] CMS Collaboration, *Measurement of the mass of the top quark in decays with a J/ψ meson in pp collisions at 8 TeV*, [JHEP **12** \(2016\) 123](#), arXiv: [1608.03560 \[hep-ex\]](#) (cit. on pp. 2, 18).
- [8] ATLAS Collaboration, *Measurement of the top quark mass in the $t\bar{t} \rightarrow \text{lepton} + \text{jets}$ channel from $\sqrt{s} = 8$ TeV ATLAS data and combination with previous results*, [Eur. Phys. J. C **79** \(2019\) 290](#), arXiv: [1810.01772 \[hep-ex\]](#) (cit. on pp. 2, 18).
- [9] CMS Collaboration, *Measurement of the top quark mass using proton-proton data at $\sqrt{s}=7$ and 8 TeV*, [Phys. Rev. D **93** \(2016\) 072004](#) (cit. on pp. 2, 18).
- [10] The Tevatron Electroweak Working Group, *Combination of CDF and D0 results on the mass of the top quark using up to 9.7 fb^{-1} at the Tevatron*, (2016), arXiv: [1608.01881](#) (cit. on pp. 2, 18).
- [11] ATLAS Collaboration, *The ATLAS Experiment at the CERN Large Hadron Collider*, [JINST **3** \(2008\) S08003](#) (cit. on p. 2).
- [12] ATLAS Collaboration, *ATLAS Insertable B-Layer Technical Design Report*, ATLAS-TDR-19, 2010, URL: <https://cds.cern.ch/record/1291633> (cit. on p. 3), Addendum: ATLAS-TDR-19-ADD-1, 2012, URL: <https://cds.cern.ch/record/1451888>.
- [13] B. Abbott et al., *Production and Integration of the ATLAS Insertable B-Layer*, [JINST **13** \(2018\) T05008](#), arXiv: [1803.00844 \[physics.ins-det\]](#) (cit. on p. 3).
- [14] ATLAS Collaboration, *Performance of the ATLAS trigger system in 2015*, [Eur. Phys. J. C **77** \(2017\) 317](#), arXiv: [1611.09661 \[hep-ex\]](#) (cit. on p. 3).
- [15] ATLAS Collaboration, *Luminosity determination in pp collisions at $\sqrt{s} = 13$ TeV using the ATLAS detector at the LHC*, ATLAS-CONF-2019-021, 2019, URL: <https://cds.cern.ch/record/2677054> (cit. on pp. 3, 13).
- [16] ATLAS Collaboration, *Topological cell clustering in the ATLAS calorimeters and its performance in LHC Run I*, [Eur. Phys. J. C **77** \(2017\) 490](#), arXiv: [1603.02934 \[hep-ex\]](#) (cit. on p. 3).
- [17] M. Cacciari, G. Salam and G. Soyez, *The anti- k_t jet clustering algorithm*, [JHEP **04** \(2008\) 063](#), arXiv: [0802.1189 \[hep-ph\]](#) (cit. on p. 3).
- [18] ATLAS Collaboration, *Jet energy scale measurements and their systematic uncertainties in proton–proton collisions at $\sqrt{s} = 13$ TeV with the ATLAS detector*, [Phys. Rev. D **96** \(2017\) 072002](#), arXiv: [1703.09665 \[hep-ex\]](#) (cit. on pp. 3, 14).

- [19] ATLAS Collaboration, *Performance of missing transverse momentum reconstruction with the ATLAS detector using proton–proton collisions at $\sqrt{s} = 13$ TeV*, *Eur. Phys. J. C* **78** (2018) 903, arXiv: [1802.08168 \[hep-ex\]](#) (cit. on pp. 3, 14).
- [20] ATLAS Collaboration, *Performance of electron and photon triggers in ATLAS during LHC Run 2*, (2019), arXiv: [1909.00761 \[hep-ex\]](#) (cit. on p. 4).
- [21] ATLAS Collaboration, *Performance of the ATLAS trigger system in 2015*, *Eur. Phys. J. C* **77** (2017) 317, arXiv: [1611.09661 \[hep-ex\]](#) (cit. on p. 4).
- [22] ATLAS Collaboration, *Electron reconstruction and identification in the ATLAS experiment using the 2015 and 2016 LHC proton–proton collision data at $\sqrt{s} = 13$ TeV*, *Eur. Phys. J.* **79** (2019) 639, arXiv: [1902.04655 \[hep-ex\]](#) (cit. on pp. 4, 13, 14).
- [23] ATLAS Collaboration, *Muon reconstruction performance of the ATLAS detector in proton–proton collision data at $\sqrt{s} = 13$ TeV*, *Eur. Phys. J. C* **76** (2016) 292, arXiv: [1603.05598 \[hep-ex\]](#) (cit. on pp. 4, 13).
- [24] ATLAS Collaboration, *Performance of pile-up mitigation techniques for jets in pp collisions at $\sqrt{s} = 8$ TeV using the ATLAS detector*, *Eur. Phys. J. C* **76** (2016) 581, arXiv: [1510.03823 \[hep-ex\]](#) (cit. on pp. 4, 14).
- [25] ATLAS Collaboration, *Measurements of b-jet tagging efficiency with the ATLAS detector using $t\bar{t}$ events at $\sqrt{s} = 13$ TeV*, *JHEP* **08** (2018) 089, arXiv: [1805.01845 \[hep-ex\]](#) (cit. on pp. 4, 14).
- [26] ATLAS Collaboration, *Estimation of non-prompt and fake lepton backgrounds in final states with top quarks produced in proton-proton collisions at $\sqrt{s} = 8$ TeV with the ATLAS detector*, ATLAS-CONF-2014-058, 2014, URL: <https://cds.cern.ch/record/1951336> (cit. on p. 5).
- [27] ATLAS Collaboration, *The ATLAS Simulation Infrastructure*, *Eur. Phys. J. C* **70** (2010) 823, arXiv: [1005.4568](#) (cit. on p. 5).
- [28] S. Agostinelli et al., *GEANT4: A Simulation toolkit*, *Nucl. Instrum. Meth. A* **506** (2003) 250 (cit. on p. 5).
- [29] ATLAS Collaboration, *The simulation principle and performance of the ATLAS fast calorimeter simulation FastCaloSim*, ATL-PHYS-PUB-2010-013, 2010, URL: <https://cds.cern.ch/record/1300517> (cit. on p. 5).
- [30] T. Sjöstrand, S. Mrenna and P. Z. Skands, *A brief introduction to PYTHIA 8.1*, *Comput. Phys. Commun.* **178** (2008) 852, arXiv: [0710.3820 \[hep-ph\]](#) (cit. on pp. 5, 6).
- [31] A.D. Martin et al., *Parton distributions for the LHC*, *Eur. Phys. J. C* **63** (2009) 189, arXiv: [0901.0002 \[hep-ph\]](#) (cit. on p. 5).
- [32] A.D. Martin et al., *Uncertainties on α_S in global PDF analyses and implications for predicted hadronic cross sections*, *Eur. Phys. J. C* **64** (2009) 653, arXiv: [0905.3531 \[hep-ph\]](#) (cit. on p. 5).
- [33] ATLAS Collaboration, *ATLAS tunes of PYTHIA 6 and Pythia 8 for MC11*, ATL-PHYS-PUB-2011-009, 2011, URL: <https://cds.cern.ch/record/1363300> (cit. on p. 5).
- [34] ATLAS Collaboration, *Measurements of charge and CP asymmetries in b-hadron decays using top-quark events collected by the ATLAS detector in pp collisions at $\sqrt{s} = 8$ TeV*, *JHEP* **02** (2017) 071, arXiv: [1610.07869 \[hep-ex\]](#) (cit. on p. 5).
- [35] S. Frixione, P. Nason and G. Ridolfi, *A Positive-weight next-to-leading-order Monte Carlo for heavy flavour hadroproduction*, *JHEP* **09** (2007) 126, arXiv: [0707.3088](#) (cit. on p. 6).

- [36] P. Nason, *A New method for combining NLO QCD with shower Monte Carlo algorithms*, **JHEP** **11** (2004) 040, arXiv: [hep-ph/0409146](#) (cit. on p. 6).
- [37] S. Alioli, P. Nason, C. Oleari and E. Re, *A general framework for implementing NLO calculations in shower Monte Carlo programs: the POWHEG BOX*, **JHEP** **06** (2010) 043, arXiv: [1002.2581 \[hep-ph\]](#) (cit. on p. 6).
- [38] R. D. Ball et al., *Parton distributions for the LHC Run II*, **JHEP** **04** (2015) 040, arXiv: [1410.8849 \[hep-ph\]](#) (cit. on p. 6).
- [39] S. Frixione, E. Laenen, P. Motylinski and B. R. Webber, *Angular correlations of lepton pairs from vector boson and top quark decays in Monte Carlo simulations*, **JHEP** **04** (2007) 081, arXiv: [hep-ph/0702198](#) (cit. on p. 6).
- [40] ATLAS Collaboration, *ATLAS Pythia 8 tunes to 7 TeV data*, ATL-PHYS-PUB-2014-021, 2014, URL: <https://cds.cern.ch/record/1966419> (cit. on p. 6).
- [41] D. J. Lange, *The EvtGen particle decay simulation package*, **Nucl. Instrum. Meth. A** **462** (2001) 152 (cit. on p. 6).
- [42] M. Czakon and A. Mitov, *Top++: A program for the calculation of the top-pair cross-section at hadron colliders*, **Comput. Phys. Commun.** **185** (2014) 2930, arXiv: [1112.5675 \[hep-ph\]](#) (cit. on p. 6).
- [43] M. Cacciari, M. Czakon, M. Mangano, A. Mitov and P. Nason, *Top-pair production at hadron colliders with next-to-next-to-leading logarithmic soft-gluon resummation*, **Phys. Lett. B** **710** (2012) 612, arXiv: [1111.5869 \[hep-ph\]](#) (cit. on p. 6).
- [44] P. Bärnreuther, M. Czakon and A. Mitov, *Percent Level Precision Physics at the Tevatron: First Genuine NNLO QCD Corrections to $q\bar{q} \rightarrow t\bar{t}$* , **Phys. Rev. Lett.** **109** (2012) 132001, arXiv: [1204.5201 \[hep-ph\]](#) (cit. on p. 6).
- [45] M. Czakon and A. Mitov, *NNLO corrections to top-pair production at hadron colliders: the all-fermionic scattering channels*, **JHEP** **12** (2012) 54, arXiv: [1207.0236 \[hep-ph\]](#) (cit. on p. 6).
- [46] M. Czakon and A. Mitov, *NNLO corrections to top-pair production at hadron colliders: the quark-gluon reaction*, **JHEP** **01** (2013) 80, arXiv: [1210.6832 \[hep-ph\]](#) (cit. on p. 6).
- [47] M. Czakon, P. Fiedler and A. Mitov, *Total Top-Quark Pair-Production Cross Section at Hadron Colliders Through $O(\alpha_s^4)$* , **Phys. Rev. Lett.** **110** (2013) 252004, arXiv: [1303.6254 \[hep-ph\]](#) (cit. on p. 6).
- [48] T. Gleisberg et al., *Event generation with SHERPA 1.1*, **JHEP** **02** (2009) 007, arXiv: [0811.4622 \[hep-ph\]](#) (cit. on p. 6).
- [49] T. Gleisberg and S. Höche, *Comix, a new matrix element generator*, **JHEP** **12** (2008) 039, arXiv: [0808.3674 \[hep-ph\]](#) (cit. on p. 6).
- [50] S. Schumann and F. Krauss, *A Parton shower algorithm based on Catani-Seymour dipole factorisation*, **JHEP** **03** (2008) 038, arXiv: [0709.1027 \[hep-ph\]](#) (cit. on p. 6).
- [51] S. Höche, F. Krauss, M. Schönherr and F. Siegert, *QCD matrix elements + parton showers: The NLO case*, **JHEP** **04** (2013) 027, arXiv: [1207.5030 \[hep-ph\]](#) (cit. on p. 6).
- [52] ATLAS Collaboration, *Measurements of differential cross sections of top quark pair production in association with jets in pp collisions at $\sqrt{s} = 13$ TeV using the ATLAS detector*, **JHEP** **10** (2018) 159, arXiv: [1802.06572 \[hep-ex\]](#) (cit. on p. 6).

- [53] S. Frixione, E. Laenen, P. Motylinski, B. R. Webber and C. D. White, *Single-top hadroproduction in association with a W boson*, [JHEP **07** \(2008\) 029](#), arXiv: [0805.3067 \[hep-ph\]](#) (cit. on pp. 6, 16).
- [54] P. Artoisenet, R. Frederix, O. Mattelaer and R. Rietkerk, *Automatic spin-entangled decays of heavy resonances in Monte Carlo simulations*, [JHEP **03** \(2013\) 015](#), arXiv: [1212.3460 \[hep-ph\]](#) (cit. on p. 6).
- [55] T. Sjöstrand, S. Mrenna and P. Skands, *PYTHIA 6.4 Physics and Manual*, [JHEP **05** \(2006\) 036](#), arXiv: [hep-ph/0603175 \[hep-ph\]](#) (cit. on p. 6).
- [56] P. Z. Skands, *Tuning Monte Carlo Generators: The Perugia Tunes*, [Phys. Rev. D **82** \(2010\) 074018](#), arXiv: [1005.3457](#) (cit. on p. 6).
- [57] N. Kidonakis, *Two-loop soft anomalous dimensions for single top quark associated production with a W- or H-*, [Phys. Rev. D **82** \(2010\) 054018](#), arXiv: [1005.4451 \[hep-ph\]](#) (cit. on pp. 6, 16).
- [58] N. Kidonakis, *NNLL resummation for s-channel single top quark production*, [Phys. Rev. D **81** \(2010\) 054028](#), arXiv: [1001.5034 \[hep-ph\]](#) (cit. on pp. 6, 16).
- [59] N. Kidonakis, *Next-to-next-to-leading-order collinear and soft gluon corrections for t-channel single top quark production*, [Phys. Rev. D **83** \(2011\) 091503](#), arXiv: [1103.2792 \[hep-ph\]](#) (cit. on pp. 6, 16).
- [60] M. Bahr et al., *Herwig++ Physics and Manual*, [Eur. Phys. J. C **58** \(2008\) 639](#), arXiv: [0803.0883 \[hep-ph\]](#) (cit. on p. 7).
- [61] J. Bellm et al., *Herwig 7.0/Herwig++ 3.0 release note*, [Eur. Phys. J. C **76** \(2016\) 196](#), arXiv: [1512.01178 \[hep-ph\]](#) (cit. on p. 7).
- [62] B. Andersson, G. Gustafson, G. Ingelman and T. Sjostrand, *Parton Fragmentation and String Dynamics*, [Phys. Rept. **97** \(1983\) 145](#) (cit. on p. 7).
- [63] M. Bowler, *e^+e^- Production of Heavy Quarks in the String Model*, [Z. Phys. C **11** \(1981\) 169](#) (cit. on p. 7).
- [64] P. Skands, S. Carrazza and J. Rojo, *Tuning PYTHIA 8.1: the Monash 2013 Tune*, [Eur. Phys. J. C **74** \(2014\) 3024](#), arXiv: [1404.5630 \[hep-ph\]](#) (cit. on p. 7).
- [65] G. Corcella and V. Drollinger, *Bottom-quark fragmentation: Comparing results from tuned event generators and resummed calculations*, [Nucl. Phys. B **730** \(2005\) 82](#) (cit. on p. 7).
- [66] G. Corcella and F. Mescia, *A Phenomenological Study of Bottom Quark Fragmentation in Top Quark Decay*, [Eur. Phys. J. C **65** \(2010\) 171](#) (cit. on p. 7).
- [67] G. Corcella and F. Mescia, *Erratum to: A phenomenological study of bottom-quark fragmentation in top-quark decay*, [Eur. Phys. J. C **68** \(2010\) 687](#) (cit. on p. 7).
- [68] G. Corcella, R. Franceschini and D. Kim, *Fragmentation Uncertainties in Hadronic Observables for Top-quark Mass Measurements*, [Nucl. Phys. B **929** \(2018\) 485](#) (cit. on p. 7).
- [69] ALEPH Collaboration, *Study of the fragmentation of b quarks into B mesons at the Z peak*, [Phys. Lett. B **512** \(2001\) 30](#), arXiv: [hep-ex/0106051](#) (cit. on p. 7).
- [70] DELPHI Collaboration, *A study of the b-quark fragmentation function with the DELPHI detector at LEP I and an averaged distribution obtained at the Z Pole*, [Eur. Phys. J. C **71** \(2011\) 1557](#), arXiv: [1102.4748 \[hep-ex\]](#) (cit. on p. 7).
- [71] OPAL Collaboration, *Inclusive analysis of the b quark fragmentation function in Z decays at LEP*, [Eur. Phys. J. C **29** \(2003\) 463](#), arXiv: [hep-ex/0210031 \[hep-ex\]](#) (cit. on p. 7).

- [72] SLD Collaboration, *Precise Measurement of the b -Quark Fragmentation Function in Z^0 Boson Decays*, *Phys. Rev. Lett.* **84** (2000) 4300 (cit. on p. 7).
- [73] A. Buckley, H. Hoeth, H. Lacker, H. Schulz and J. E. Von Seggern, *Systematic event generator tuning for the LHC*, *Eur. Phys. J. C* **65** (2010) 331, arXiv: [0907.2973 \[hep-ph\]](#) (cit. on p. 7).
- [74] A. Buckley et al., *Rivet user manual*, *Comput. Phys. Commun.* **184** (2013) 2803, arXiv: [1003.0694 \[hep-ph\]](#) (cit. on p. 7).
- [75] Heavy Flavour Averaging Group (HFAG), *Averages of b -hadron, c -hadron, and τ -lepton properties as of summer 2014*, (2014), arXiv: [1412.7515 \[hep-ex\]](#) (cit. on p. 7).
- [76] E. Lohrmann, *A Summary of Charm Hadron Production Fractions*, (2011), arXiv: [1112.3757 \[hep-ex\]](#) (cit. on pp. 7, 8).
- [77] DELPHI Collaboration, *Measurement of the semileptonic b branching fractions and average b mixing parameter in Z decays*, *Eur. Phys. J. C* **20** (2001) 455, arXiv: [hep-ex/0105080](#) (cit. on p. 7).
- [78] LEP Electroweak Working Group, and the SLD Heavy Flavour and Electroweak Groups, *Input Parameters for the LEP Electroweak Heavy Flavour Results for Summer 2001 Conferences, LEPHF 2001-01* (see <https://www.cern.ch/LEPEWWG/heavy/>) used for the Combination of Preliminary Electroweak Measurements and Constraints on the Standard Model, (2001) (cit. on p. 7).
- [79] CLEO Collaboration, *Flavor-Specific Inclusive B Decays to Charm*, *Phys. Rev. Lett.* **80** (1998) 1150, arXiv: [hep-ex/9710028 \[hep-ex\]](#) (cit. on p. 7).
- [80] CLEO Collaboration, *Measurements of $B \rightarrow D_s^+ X$ decays*, *Phys. Rev. D* **53** (1996) 4734 (cit. on p. 7).
- [81] CLEO Collaboration, *Study of flavor-tagged baryon production in B decay*, *Phys. Rev. D* **55** (1997) 13 (cit. on p. 7).
- [82] ALEPH Collaboration, *Observation of doubly-charmed B decays at LEP*, *Eur. Phys Journal C* **4** (1998) 387 (cit. on p. 7).
- [83] R. D. Cousins, *Generalization of Chisquare Goodness-of-Fit Test for Binned Data Using Saturated Models , with Application to Histograms*, (2013), URL: <https://www.semanticscholar.org/paper/Generalization-of-Chisquare-Goodness-ofFit-Test-for-Cousins/f816576fdb04547e4db2f72656136060849b3ecf> (cit. on p. 12).
- [84] G. Avoni et al., *The new LUCID-2 detector for luminosity measurement and monitoring in ATLAS*, *JINST* **13** (2018) P07017 (cit. on p. 13).
- [85] ATLAS Collaboration, *Jet Calibration and Systematic Uncertainties for Jets Reconstructed in the ATLAS Detector at $\sqrt{s} = 13\text{TeV}$* , ATL-PHYS-PUB-2015-015 (2015), URL: <https://cds.cern.ch/record/2037613> (cit. on p. 14).
- [86] ATLAS Collaboration, *Measurement of b -tagging efficiency of c -jets in $t\bar{t}$ events using a likelihood approach with the ATLAS detector*, ATLAS-CONF-2018-001, 2018, URL: <https://cds.cern.ch/record/2306649> (cit. on p. 14).
- [87] ATLAS Collaboration, *Calibration of light-flavour b -jet mistagging rates using ATLAS proton–proton collision data at $\sqrt{s} = 13\text{ TeV}$* , ATLAS-CONF-2018-006, 2018, URL: <https://cds.cern.ch/record/2314418> (cit. on p. 14).
- [88] ATLAS Collaboration, *Measurements of top-quark pair differential and double-differential cross-sections in the l +jets channel with pp collisions at $\sqrt{s} = 13\text{ TeV}$ using the ATLAS detector*, (2019), arXiv: [1908.07305 \[hep-ex\]](#) (cit. on p. 15).

- [89] S. Argyropoulos and T. Sjöstrand, *Effects of color reconnection on $t\bar{t}$ final states at the LHC*, [JHEP **11** \(2014\) 043](#), arXiv: [1407.6653 \[hep-ph\]](#) (cit. on p. 15).
- [90] ATLAS Collaboration, *Simulation of top-quark production for the ATLAS experiment at $\sqrt{s} = 13$ TeV*, ATL-PHYS-PUB-2016-004, 2016, URL: <https://cds.cern.ch/record/2120417> (cit. on p. 15).
- [91] ATLAS Collaboration, *Measurement of jet shapes in top-quark pair events at $\sqrt{s} = 7$ TeV using the ATLAS detector*, [Eur. Phys. J. C **73** \(2013\) 2676](#) (cit. on p. 16).
- [92] S. Mrenna and P. Skands, *Automated parton-shower variations in Pythia 8*, [Phys. Rev. D **94** \(2016\) 074005](#), arXiv: [1605.08352 \[hep-ph\]](#) (cit. on p. 16).
- [93] ATLAS Collaboration, *Multi-boson simulation for 13 TeV ATLAS analyses*, ATL-PHYS-PUB-2016-002, 2016, URL: <https://cds.cern.ch/record/2119986> (cit. on p. 16).